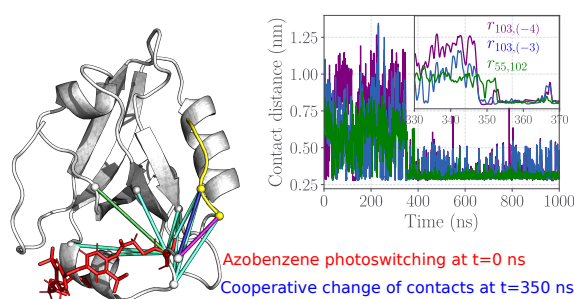


Nonequilibrium Modeling of the Elementary Step in PDZ3 Allosteric Communication

Ahmed A. A. I. Ali,^{1, a)} Adnan Gulzar,^{1, a)} Steffen Wolf,¹ and Gerhard Stock^{1, b)}
 Biomolecular Dynamics, Institute of Physics, University of Freiburg, 79104 Freiburg,
 Germany

(Dated: 19 September 2022)

ABSTRACT: While allostery is of paramount importance for protein signaling and regulation, the underlying dynamical process of allosteric communication is not well understood. PDZ3 domain represents a prime example of an allosteric single-domain protein, as it features a well-established long-range coupling between the C-terminal α_3 -helix and ligand binding. In an intriguing experiment, Hamm and coworkers employed photoswitching of the α_3 -helix to initiate a conformational change of PDZ3 that propagates from the C-terminus to the bound ligand within 200 ns. Performing extensive nonequilibrium molecular dynamics simulations, the modeling of the experiment reproduces the measured timescales and reveals a detailed picture of the allosteric communication in PDZ3. In particular, a correlation analysis identifies a network of contacts connecting the α_3 -helix and the core of the protein, which move in a concerted manner. Representing a one-step process and involving direct α_3 -ligand contacts, this cooperative transition is considered as elementary step in the propagation of conformational change.



INTRODUCTION

Allostery is one of the most important mechanisms of biomolecular regulation and signal transduction.^{1–9} While commonly this term is meant to describe the communication between distal domains of large macromolecules, it has been suggested that even relatively small single-domain proteins exhibit allosteric properties.² PDZ domains, for example, are well-established and structurally conserved protein interaction modules involved in the regulation of multiple receptor-coupled signal transduction processes, but at the same time have also been studied extensively as isolated model systems of allosteric communication.^{10–13} They share a common fold, which consists of two α -helices and six β -strands, with the second α -helix and the second β -strand forming the canonical ligand binding groove (Fig. 1), and generally bind the C-terminus of their targets.

Notably, the NMR study of Petit et al.¹¹ showed that the removal of a short α -helix at the C-terminal of PDZ3 reduces ligand affinity by a factor of 21, thus revealing an allosteric communication between ligand binding and

C-terminal dynamics. In this way, PDZ3 can be regarded as one of the smallest allosteric proteins, in the sense that both the active site (the α_3 -helix) and the allosteric site (the binding pocket) are clearly defined. Notwithstanding numerous experimental and computational studies of PDZ domains (see Refs. 10–21 for a rather incomplete selection), however, it is still not well understood how exactly a local perturbation propagates through the protein in space and time to a distal site. This is due to the typically small local structural changes of an allosteric signal which are challenging to observe in experiments,²² and also because of the timescale limitations of molecular dynamics (MD) simulations.^{23–26}

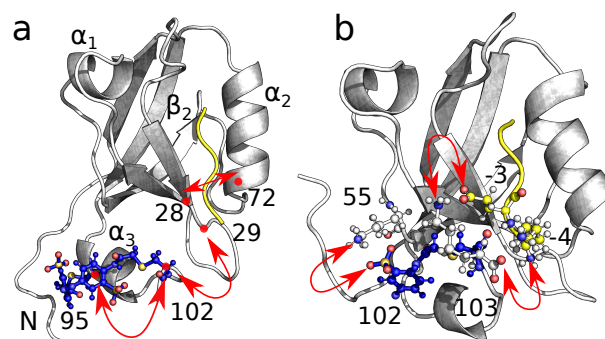


FIG. 1. Photoswitchable PDZ3 domain studied by Bozovic et al.²⁷ Upon *cis*-to-*trans* isomerization, the azobenzene photo-switch (blue) unfolds the α_3 -helix of the system and initiates an allosteric transition that changes the binding affinity of the ligand (yellow). Panel (a) shows the *cis* state of the system and indicates main secondary structural elements as well as C_α -distances $d_{95,102}$, $d_{28,72}$ and $d_{29,102}$ discussed in the text. Panel (b) shows the *trans* state with its three stabilizing salt bridges Azo102-Lys55, Lys103-Lys(-4) and Lys103-Glu(-3). Residues are numbered from 1 to 103 for the protein and from -4 to 0 for the ligand.

To facilitate a real-time study of the underlying al-

^{a)} A. Ali and A. Gulzar contributed equally to this work.

^{b)} Electronic mail: stock@physik.uni-freiburg.de

losteric transition in PDZ domains, Hamm and coworkers implemented an azobenzene photoswitch that impulsively perturb the protein (e.g., by causing the unbinding of the ligand), and monitored the subsequent structural evolution of the system via time-resolved vibrational spectroscopy.^{27–31} As a main result, they found for PDZ2 that the conformational rearrangement of the photoswitchable protein occurs on multiple timescales from pico- to microseconds in a highly nonexponential manner.²⁰ Accompanying MD studies of the nonequilibrium dynamics reproduced these findings and revealed a quite complex structural reorganization of the system.^{32,33} Most recently, Bozovic et al.²⁷ employed photoswitching of the α_3 -helix to initiate a conformational change of PDZ3 that propagates from the α_3 -helix to the binding pocket of the ligand. They found a timescale of 4 to 6 ns for the enforced unfolding of the α_3 -helix, as well as 200 ns for the time it takes for the allosteric signal to reach the ligand.

To aid the interpretation of these experiments and to unravel the atomistic mechanism of the putative allosteric transition in PDZ3, in this work we perform extensive all-atom explicit-solvent MD simulations of photoswitchable PDZ3. Aiming to directly model the experiment of Bozovic et al.,²⁷ we employ a potential-energy surface switching method³⁴ to collect $100 \times 1 \mu\text{s}$ -long nonequilibrium trajectories of the photoinduced conformational change of PDZ3. In excellent agreement with experiment, we find that the initial unfolding of the α_3 -helix occurs on a 5 ns timescale and causes a population shift of protein-attached and protein-separated conformations of the α_3 -helix, which in turn triggers a long-range conformational transition involving the ligand on a timescale of about 300 ns.

RESULTS

Similarity of photoswitchable and wild-type PDZ3

In the experiment of Bozovic et al.,²⁷ the azobenzene photoswitch was attached to the side-chains of residues 95 and 102 of the α_3 -helix. In this way, the end-to-end distance of azobenzene in its stretched *trans* configuration accommodates a stable α_3 -helix, while the twisted *cis* configuration destabilizes the helix. To verify that the photoswitchable PDZ3 represents a suitable model for the wild-type protein, we performed $8 \times 10 \mu\text{s}$ -long equilibrium MD simulations of the *cis* and the *trans* systems, based on a crystal structure³⁵ (PDB entry 1TP5) and using the GROMACS v2020 software package³⁶ and the Amber99SB*ILDN force field,^{37–39} see SI Methods. Calculating the time-dependent root mean square displacement (RMSD) matrix of the *cis* and the wild-type trajectories, Fig. S1 shows that the C_α -RMSD of the full protein never exceeds 2.65 Å throughout the $1 \mu\text{s}$ time evolution shown. With an average of 1.45 Å, the RMSD can be regarded as a sufficient similarity between photoswitchable and wild-type protein. As a further validation of the simulation model, we calculated the side-chain methyl groups fluctuations⁴⁰ as measured by the NMR

order parameters S^2 of Petit et al.,¹¹ see SI Methods. Comparing S^2 values obtained from the simulation of *cis* PDZ3 and the wild-type protein as well as from experiment and wild-type simulation, we obtain good overall agreement (Fig. S1).

Structural changes of PDZ3 upon photoswitching

To get a first impression of the photoinduced conformational transition of PDZ3, we follow Buchenberg et al.³³ and consider selected interresidue C_α -distances that account for various aspects of the structural rearrangement. As a first example, Fig. 2 shows the distance $d_{95,102}$ between residues Azo95 and Azo102 bridged by the photoswitch, which reports on the length of the α_3 -helix (Fig. 1a). The distribution of $d_{95,102}$ reveals a shift of about 3 Å upon switching from the *cis* to the *trans* equilibrium state, which clearly reflects the photoinduced stretching and partial unfolding of α_3 .

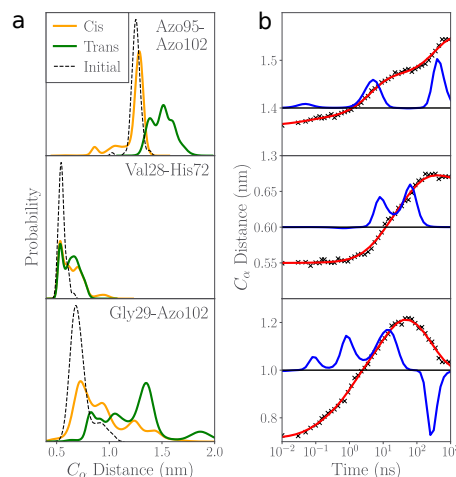


FIG. 2. Distribution (a) and time evolution (b) of three C_α -distances that describe the structural rearrangement of PDZ3: $d_{95,102}$ indicating the length of α_3 -helix, $d_{28,72}$ representing the width of the binding pocket, and $d_{29,102}$ accounting for the distance between α_3 and the core of the protein. Distributions are obtained for the *cis* and *trans* equilibrium states, as well as for the initial state of the nonequilibrium simulations. The time traces in red are fits of the MD data (black points) from the timescale analysis [Eq. (1)], and the blue lines are the resulting timescale spectra.

To study the time evolution of the system following *cis* to *trans* photoswitching, we sampled 100 statistically independent structures from the *cis* equilibrium simulations, performed at time $t = 0$ a potential-energy surface switching method,³⁴ and calculated $100 \times 1 \mu\text{s}$ -long nonequilibrium trajectories. By performing an ensemble average over these trajectories, we obtain the time-dependent mean value $\langle d(t) \rangle$ of some observable d . Using a log-scale representation of the time axis ranging from 10 ps to $1 \mu\text{s}$, Fig. 2b shows the photoinduced evolution of $\langle d_{95,102}(t) \rangle$, which is found to increase on several

timescales. To facilitate the interpretation, we perform a timescale analysis using a maximum entropy method⁴¹

$$\langle d(t) \rangle = \sum_k a_k e^{-t/\tau_k}, \quad (1)$$

where the amplitudes a_k of the multiexponential fit yield the timescale spectrum $a(\tau_k)$ of the evolution. We used 10 equally distributed timescales τ_k per decade and a regularization parameter $\lambda = 3 \times 10^{-4}$. The analysis of $\langle d_{95,102}(t) \rangle$ reveals that the sub-ps photoisomerization of azobenzene⁴² causes an elongation of the α_3 -helix on timescales of ~ 5 and 400 ns. A structural analysis (Fig. S2) shows that the short timescale reflects the initial stretching of α_3 , which is in perfect agreement with the experimental result (4 to 6 ns) of Bozovic et al.²⁷ The long timescale accounts for the structural relaxation of the α_3 -helix due to the subsequent rearrangement of PDZ3 to be discussed below.

As an indicator of how the initial stretching of the α_3 -helix affects the environment of the distal ligand of PDZ3, Fig. 2 shows the distance between Val28 in the β_2 -strand and His72 in the α_2 -helix, which accounts for the width of the binding pocket³³ (Fig. 1a). While the distributions of $d_{28,72}$ in *cis* and *trans* equilibrium states are rather similar, we find a clear increase of $\langle d_{28,72}(t) \rangle$ on timescales of ~ 8 and 60 ns. This supposed discrepancy between distributions and time evolution reflects the fact that the nonequilibrium simulations were started close to the initial structure (dotted lines in Fig. 2), and therefore exhibit a short-time relaxation to the appropriate conformational distribution.

Finally, we consider the C_α distance between Azo102 and Gly29 in the β_2 - β_3 loop as an observable that reports on the attachment of the α_3 -helix to the core of the protein (Fig. 1a). Since the alignment and the separation of α_3 to and from the protein core is believed to represent the origin of the change in ligand binding affinity,^{11,30} $d_{29,102}$ can be considered as a simple descriptor of the allosteric transition. Figure 2a shows that the distribution of $d_{29,102}$ is rather broad and exhibits a significant shift (~ 0.7 nm) of its maximum upon *cis*-to-*trans* switching. When we roughly associate distances $d_{29,102} \lesssim 1$ nm with structures where the α_3 -helix is attached to the core, and larger distances with an unattached α_3 -helix, $d_{29,102}$ suggests a decrease of 68 to 32% of attached structures when we change from *cis* to *trans*. Rather than a simple one-to-one relation of *cis* and *trans* states with an attached and separated α_3 -helix, respectively, we thus find a coexistence of both structures in both states, which undergo a population shift upon *cis* to *trans* switching.

In line with its large structural heterogeneity, the time evolution of the α_3 -core distance is found to be quite complex. $\langle d_{29,102}(t) \rangle$ first increases on several timescales (~ 0.1 , 1 and 10 ns), before it starts to decrease on a ~ 250 ns timescale. While the fast timescales again reflect the short-time relaxation of the initially prepared state, the long timescale seems to indicate the subsequent allosteric transition of PDZ3. To summarize, we

have identified a timescale of 5 ns associated with the initial stretching of the α_3 -helix, an intermediate timescale (tens of ns) that reflects the short-time relaxation of the initially prepared structural distribution, and a slow timescale (~ 300 ns) whose structural origin is to be explained next.

Correlation analysis of interresidue contacts

To identify internal coordinates that change significantly during the conformational transition, we follow recent work^{43,44} and focus on interresidue contact distances. This is for two reasons. First, although contact distances report only on near-order interactions, long-distance changes of the structure result as a consequence and are therefore included as well. Moreover, while side-chain dihedral angles may also mediate allosteric couplings,^{44,45} analyses including them showed that they are not of relevance for PDZ3. Assuming that a contact is formed if the distance r_{ij} between the closest non-hydrogen atoms of residues i and j is shorter than 4.5 \AA ,⁴⁶ we identified 403 interresidue contacts (see SI Methods). To discriminate collective motions underlying functional dynamics from uncorrelated motion, we calculated (the modulus of) the linear correlation matrix of these coordinates and rearranged this matrix in an approximately block-diagonal form. Following Diez et al.,⁴⁷ this is achieved via a community detection technique called Leiden clustering,⁴⁸ employing the Python package MoSAIC⁴⁷ and a Leiden resolution parameter $\gamma = 0.5$.

Figure 3a shows the resulting block-diagonal correlation matrix $\{\sigma_{ij}\}$, which reveals eight main blocks or clusters. Within such a cluster, the coordinates are highly correlated (i.e., on average $\sigma_{ij} \geq \gamma$), while the correlation between different clusters is low (i.e., $\sigma_{ij} < \gamma$). On the other hand, we find that $\sim 56\%$ of all coordinates (shown in the lower right square) correlate only weakly with few other coordinates. (This is, e.g., the case for stable contacts and contacts on the protein surface that form and break frequently.) These contact distances are therefore classified as noise and can be omitted in the further analysis. Finally, there are coordinates (or mini-clusters with ≤ 3 coordinates) that are not a member of a main cluster but still exhibit moderate correlation with some of the main clusters; they are shown in between the main clusters.

To illustrate the coordinates contained in the main clusters, Fig. 3b shows the corresponding contact distances inserted into the structure of PDZ3. (See Table S1 for a list of the coordinates of all clusters.) Most interestingly, we find that cluster 1 contains contacts between the α_3 -helix and the ligand as well as the core of the protein. Causing the (un)alignment of α_3 to the protein core, which in turn induces the change in ligand binding,^{11,30} these coordinates are the key to describe the allosteric transition in PDZ3. The remaining clusters, on the other hand, are found to describe interactions in different sections of PDZ3, whose motions are mostly uncorrelated to

the coordinates of cluster 1. For example, cluster 2 connects residue Phe100 of α_3 to the β_2 - β_3 loop, and cluster 3 and cluster 6 accounts for motions within the β_2 - β_3 and β_1 - β_2 loops, respectively.

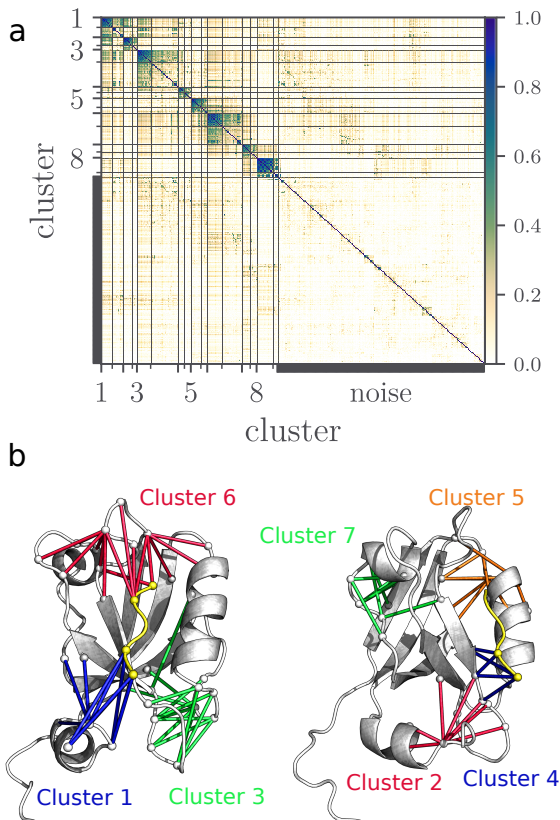


FIG. 3. (a) Block-diagonal correlation matrix obtained from Leiden clustering of 403 contact distances of PDZ3. In this way, we discriminate collective motions underlying functional dynamics (represented by the main clusters) from uncorrelated motion or noise (shown in the lower square). (b) Illustration of the contact distances (colored lines) associated with the main clusters.

Hence the Leiden correlation analysis leaves us with 11 (instead of initially 403) coordinates comprised in cluster 1, which form a network of highly correlated inter-residue contacts (Fig. 3b). The network includes 6 hydrophobic contacts, 2 hydrogen bonds, and 3 salt bridges, which connect the α_3 -helix (mostly residues Azo102 and Lys103) to ligand residues Glu(-3) and Lys(-4) and various protein residues. Selecting six representative contacts (see Fig. S4 for the other cases), Fig. 4a shows the corresponding distance distributions in the *cis* and *trans* equilibrium states. For all contacts we find a coexistence between contact-formed states (with a well-defined peak at distances $\lesssim 4.5$ Å) and contact-broken states (with a broad distribution of longer distances). We note that in *cis* the α_3 -helix is mostly stabilized by nonpolar contacts with the protein (e.g., Val28 and Tyr97 connect

to Azo102), while in *trans* polar contacts with the ligand dominate. The latter include two salt bridges between C-terminal Lys103 and the ligand residues Lys(-4) and Glu(-3), as well as a hydrogen bond between the backbone of Glu101 and the side-chain of Lys(-4). Moreover, we find the salt bridge Azo102-Lys55 between α_3 and the protein core, which exists almost exclusively in *trans*. That is, during the allosteric transition, (at least) four new contacts are formed, including three salt bridges and one hydrogen bond.

As representative examples of contacts that are formed during the photoinduced transition, Fig. 4b shows the time evolution of the salt bridges Lys55-Azo102 and Lys103-Glu(-3). In both cases, the formation occurs on two timescales of about 10 ns and 300 ns. Similar results are also obtained for the other contact distances of cluster 2 (Fig. S4). While the 10 ns timescale reflects the above discussed short-time relaxation of the initially prepared structural distribution, the long timescale (already found in Fig. 2b) can now unambiguously be associated with the allosteric transition. Assuming that the experimentally measured infrared response of the ligand is related to changes of protein-ligand contacts, the 300 ns timescale compares well to experimental ligand response time of 200 ns obtained by Bozovic et al.²⁷

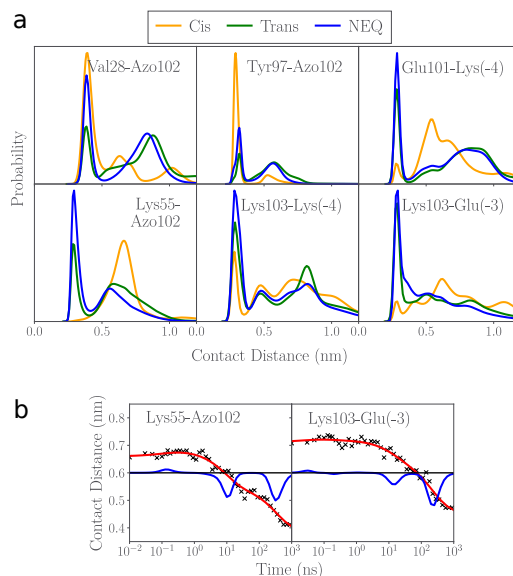


FIG. 4. (a) Distribution of various contact distances r_{ij} that mediate the allosteric transition in PDZ3, obtained for the *cis* and *trans* equilibrium states, as well as during the nonequilibrium simulations. (b) Time evolution of the salt bridge distances $r_{55,102}$ and $r_{103,(-3)}$. Time traces in red are fits of the MD data (black points) from the timescale analysis [Eq. (1)], blue lines are the resulting timescale spectra.

Cooperative mechanism of the long-range communication

The above correlation analysis indicates that the allosteric transition in PDZ3 is mediated by a network of 11 highly correlated interresidue contacts (Fig. 3b).

This raises the question if the transition proceeds sequentially (i.e., involving intermediate states) or rather in a concerted manner. To address this point, Fig. 5 shows the time evolution of the above discussed contact distances along a *single* nonequilibrium trajectory (i.e., without performing an ensemble average). Starting in the *cis* equilibrium state for times $-200 \text{ ns} \leq t \leq 0$, we find that the two *cis*-stabilizing contacts are formed (i.e., distances $r_{28,102}$ and $r_{97,102}$ fluctuate with small amplitude around 3 \AA), while the *trans*-stabilizing contacts are broken such that the corresponding distances $r_{55,102}$, $r_{101,(-4)}$, $r_{103,(-3)}$ and $r_{103,(-4)}$ fluctuate with large amplitudes. Upon *cis*-to-*trans* photoswitching at $t=0$, contacts 28-102 and 97-102 are broken, too, within tens of nanosecond. As a consequence, all distances fluctuate wildly, reflecting the large-amplitude motion of the detached α_3 -helix. At $t \sim 348 \text{ ns}$ this motion localizes abruptly, when all six contacts are formed within 5–7 ns, i.e., virtually simultaneously on the transition timescale of hundreds of nanoseconds. While contact distances $r_{102,(-4)}$, $r_{103,(-3)}$ still exhibit residual fluctuations, the other contacts are tightly closed.

Inspecting the other nonequilibrium trajectories, Fig. S5 shows that the overall picture is qualitatively similar to the above example. Of the $100 \times 1 \mu\text{s}$ -long trajectories, 44 remain in the large-amplitude state, while the other 56 undergo a concerted conformational transition, with 7 trajectories showing multiple transitions. Hence we have shown that the allosteric transition in PDZ3 proceeds in a concerted manner. That is, all contacts change almost simultaneously, similar to the cooperative mechanism that was observed in the functional dynamics of T4 lysozyme.⁴⁴ Starting in the relatively ordered *cis* state, the system becomes disordered upon *cis*-to-*trans* photoswitching and returns to an ordered state via a cooperative transition. In this way, the system follows an order-disorder-order transition, which was also observed for a photoswitchable PDZ2 domain.³³

Comparing the distance distributions from the nonequilibrium and the *trans* simulations (Fig. 4a), we notice that within $1 \mu\text{s}$ the system has not yet reached the *trans* equilibrium state, because most contacts are less likely in *trans* than during the nonequilibrium process. Similarly as shown for a photoswitchable PDZ2 domain,³³ we thus find that the final step of the allosteric transition is the slow relaxation into the new equilibrium state. Interestingly, a visual inspection of the experimental data (Fig. 3f in Ref. 27) also seems to indicate weak changes of the transient infrared spectrum at long times $t \gtrsim 1 \mu\text{s}$.

DISCUSSION AND CONCLUSIONS

In their beautiful experiment, Bozovic et al.²⁷ implemented an azobenzene photoswitch in the α_3 -helix of PDZ3, which allows to change between the *cis* state (α_3 -helix folded) and the *trans* state (α_3 -helix unfolded). The underlying idea of the experiment is that the unfolding of α_3 causes the separation of α_3 from the protein

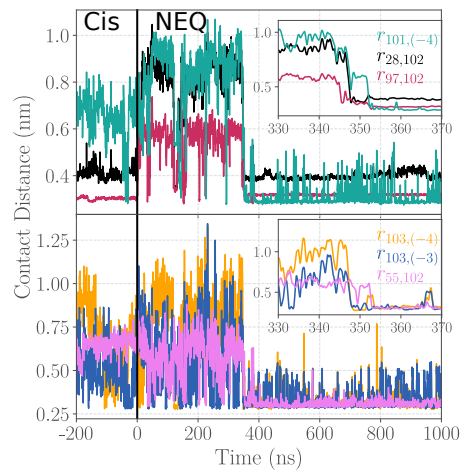


FIG. 5. Time evolution of selected contact distances along a *single* trajectory of PDZ3. For times $-200 \text{ ns} \leq t \leq 0$, the system is in the *cis* equilibrium state, and undergoes a nonequilibrium evolution following *cis*-to-*trans* photoswitching at $t=0$. For smoothing, a Gaussian filter with width $\sigma = 0.2 \text{ ns}$ was used.

core, which in turn causes a change in ligand binding affinity,^{11,30} thus establishing an allosteric coupling between α_3 and the distal ligand. Using time-resolved infrared spectroscopy, Bozovic et al. observed a timescale of 4 to 6 ns associated with the enforced unfolding of the α_3 -helix, as well as a response of the ligand within 200 ns.

Our simulation results reproduce these timescales quite accurately. We obtain a timescale of 5 ns associated with the initial stretching of the α_3 -helix (Fig. 2b), as well as a timescale of $\sim 300 \text{ ns}$ that reflects the reordering of the contact network between the α_3 -helix and the core of the protein as well as the ligand (Fig. 4b). Because the transition leads to a change of contacts formed by the ligand, it eventually can be measured via vibrational spectroscopy of the ligand. Hence we have shown that the measured timescale of 200 ns can be clearly assigned to elementary contact changes in the protein. This also aids the interpretation of previous transient infrared experiments on photoswitchable proteins,^{28,29} which too reported a typical timescale of several hundreds of nanoseconds for this process.

To identify the intramolecular interactions mediating the allosteric transition in PDZ3, we have employed a recently proposed correlation analysis of interresidue contact distances.⁴⁷ It reveals a network of highly correlated α_3 -protein contacts (Fig. 3b) that mediate a cooperative contact rearrangement in PDZ3 (Fig. 5). Involving only a one-step contact changing process, the cooperative transition can be considered as a minimal solution to transduce the information on the state of the α_3 -helix to the ligand, and represents therefore the elementary step in the allosteric communication in PDZ3. Cooperative contact rearrangements also cause large global free energy barriers that offer a plausible explanation why the often

tiny structural changes in allostery can be stabilized in spite of the presence of thermal fluctuations and noise.

Allosteric phenomena in PDZ domains (and in particular in PDZ3) have been debated for long.^{14–21} Nonetheless, our simulation of a specific experiment on PDZ3 has revealed several new and in part unexpected findings. To begin with, this concerns the existence of direct contacts between the α_3 -helix and the ligand (Fig. 4a). While the centers of mass of α_3 and the ligand are on average separated by about 1.5 nm, the long side-chains of Lys103, Azo102, Glu(3) and Lys(-4) nevertheless facilitate such contacts. They are formed in particular during the cooperative transition (Fig. 5), but may also occur in the *trans* state. Our results are in contrast to the NMR study of Petit et al.,¹¹ which excluded the possibility of direct α_3 -ligand contacts. However, they used a different ligand (NYKQTSV instead of KETWV used here) and their PDZ3 was one amino acid shorter than ours (i.e., it misses Lys103 which is involved in several contacts). We also note that direct α_3 -ligand contacts were discussed for the slightly longer ligand KKETWV⁴⁹ and for a PDZ3 domains with a longer C-terminus.^{50,51} Hence we conclude that the existence of direct contacts in PDZ3 are specific to the considered version of protein and ligand.

Recognizing that direct contacts between the putative active site (the α_3 -helix) and the allosteric site (the binding pocket) may cause at least in part the observed binding affinity change, one may question if the notion of allostery is still adequate here. On the other hand, we expect that the main finding, i.e., that allosteric communication is mediated through a concerted conformational transition that involves numerous simultaneous contact changes, prevails also in the absence of direct contacts and therefore represents a general result. For example, Post et al.⁴⁴ found a quite similar scenario for the allosteric coupling in T4 lysozyme.

A further complication revealed by our analysis is that there is no simple one-to-one relation of the *cis* and *trans* states of PDZ3 with the attachment and the separation of α_3 , respectively. Rather the calculations of the distribution of the C_α -distance $d_{29,102}$ (Fig. 2a) and the α_3 -ligand contact distances (Fig. 4a) reveal the coexistence of attached and separated structures in both states. We obtain a population shift of 68 to 32% of attached structures when we change from *cis* to *trans*, while we find on average 51% during our nonequilibrium simulations (Fig. S3). Interestingly, this dynamical heterogeneity of α_3 occurs also in the wild-type system, where the attached structures persist 45% of the time (Fig. S3). Unfortunately, existing NMR¹¹ or mutational²¹ studies do not include the α_3 -helix, which could confirm this effect.

Allosteric interactions have been commonly described by network models, which may be based on statistical inference,¹⁴ correlations,⁵² forces,⁵³ energy transfer,¹⁸ electrostatic interactions¹⁹ and many variants of thereof. While in this work we also have constructed a correlation matrix reflecting allosteric interactions, our work differs from common network approaches in two important as-

pects. First, instead of calculating all interresidue correlations using Cartesian C_α -coordinates, we directly focus on interresidue contacts that change during the allosteric transition. For the considered conformational rearrangement in PDZ3, the block diagonalization of the contact distances yielded a single cluster containing highly correlated α_3 -protein contacts (Fig. 3b), indicating that only a small part of the protein is involved in the allosteric transition.

Second, rather than describing allostery via the interpretation of some network model, we have directly simulated the allosteric transition using nonequilibrium MD, and employed the correlation analysis merely for the interpretation of the simulations. While such an approach is desirable, we admit that it will be limited to rather small allosteric systems. On the other hand, by a comparison to our MD simulations, we are now in a position to test the validity and potential of various network models, which may then facilitate the study of larger proteins.

Acknowledgments

The authors thank Andrew L. Lee for providing experimental order parameters, and Peter Hamm and his group as well as Georg Diez, Emanuel Dorbath, Daniel Nagel and Matthias Post for numerous instructive and helpful discussions. This work has been supported by the Deutsche Forschungsgemeinschaft (DFG) via the Research Unit FOR 5099 "Reducing complexity of nonequilibrium" (project No. 431945604). The authors acknowledge support by the High Performance and Cloud Computing Group at the Zentrum für Datenverarbeitung of the University of Tübingen and the Rechenzentrum of the University of Freiburg, the state of Baden-Württemberg through bwHPC and the DFG through Grant Nos. INST 37/935-1 FUGG (RV bw161016) and INST 39/963-1 FUGG (RV bw18A004).

Supporting Information Available:

Methods, 1 table, and 5 figures.

- ¹S. J. Wodak et al., Allostery in its many disguises: From theory to applications, *Structure* **27**, 566 (2019).
- ²K. Gunasekaran, B. Ma, and R. Nussinov, Is allostery an intrinsic property of all dynamic proteins?, *Proteins* **57**, 433 (2004).
- ³I. Bahar, C. Chennubhotla, and D. Tobi, Intrinsic dynamics of enzymes in the unbound state and relation to allosteric regulation, *Curr. Opin. Struct. Biol.* **17**, 633 (2007).
- ⁴Q. Cui and M. Karplus, Allostery and cooperativity revisited, *Prot. Sci.* **17**, 1295 (2008).
- ⁵J.-P. Changeux, Allostery and the Monod-Wyman-Changeux model after 50 years, *Ann. Rev. Biophys.* **41**, 103 (2012).
- ⁶T. C. B. McLeish, T. L. Rodgers, and M. R. Wilson, Allostery without conformational change: modelling protein dynamics at multiple scales, *Phys. Biol.* **10**, 056004 (2013).
- ⁷H. N. Motlagh, J. O. Wrabl, J. Li, and V. J. Hilser, The ensemble nature of allostery, *Nature (London)* **508**, 331 (2014).
- ⁸C. J. Tsai and R. Nussinov, A Unified View of "How Allostery Works", *PLoS Comput. Biol.* **10** (2014).
- ⁹D. Thirumalai, C. Hyeon, P. I. Zhuravlev, and G. H. Lorimer, Symmetry, rigidity, and allosteric signaling: From monomeric proteins to molecular machines, *Chem. Rev.* **119**, 6788 (2019).
- ¹⁰E. Fuentes, C. Der, and A. Lee, Ligand-dependent dynamics and intramolecular signaling in a PDZ domain, *J. Mol. Biol.* **335**, 1105 (2004).

- ¹¹C. M. Petit, J. Zhang, P. J. Sapienza, E. J. Fuentes, and A. L. Lee, Hidden dynamic allostery in a PDZ domain, *Proc. Natl. Acad. Sci. USA* **106**, 18249 (2009).
- ¹²H.-J. Lee and J. J. Zheng, Pdz domains and their binding partners: structure, specificity, and modification., *Cell communication and signaling : CCS* **8**, 8 (2010).
- ¹³F. Ye and M. Zhang, Structures and target recognition modes of PDZ domains: recurring themes and emerging pictures, *Biochem. J.* **455**, 1 (2013).
- ¹⁴S. W. Lockless and R. Ranganathan, Evolutionarily conserved pathways of energetic connectivity in protein families, *Science* **286**, 295 (1999).
- ¹⁵N. Ota and D. A. Agard, Intramolecular signaling pathways revealed by molecular anisotropic thermal diffusion, *J. Mol. Biol.* **351**, 345 (2005).
- ¹⁶Y. Kong and M. Karplus, Signaling pathways of PDZ2 domain: A molecular dynamics interaction correlation analysis, *Proteins* **74**, 145 (2009).
- ¹⁷Z. N. Gerek and S. B. Ozkan, Change in Allosteric Network Affects Binding Affinities of PDZ Domains: Analysis through Perturbation Response Scanning, *PLoS Comput. Biol.* **7** (2011).
- ¹⁸T. Ishikura, Y. Iwata, T. Hatano, and T. Yamato, Energy exchange network of inter-residue interactions within a thermally fluctuating protein molecule: A computational study, *J. Comput. Chem.* **36**, 1709 (2015).
- ¹⁹A. Kumawat and S. Chakrabarty, Hidden electrostatic basis of dynamic allostery in a PDZ domain, *Proc. Natl. Acad. Sci. USA* **114**, E5825 (2017).
- ²⁰G. Stock and P. Hamm, A nonequilibrium approach to allosteric communication, *Phil. Trans. B* **373**, 20170187 (2018).
- ²¹A. J. Faure, J. Domingo, J. M. Schmiedel, C. Hidalgo-Carcedo, G. Diss, and B. Lehner, Mapping the energetic and allosteric landscapes of protein binding domains, *Nature* **604**, 175 (2022).
- ²²S. Brüscheiler, P. Schanda, K. Klobner, B. Brutscher, G. Kontaxis, R. Konrat, and M. Tollinger, Direct observation of the dynamic process underlying allosteric signal transmission, *J. Am. Chem. Soc.* **131**, 3063 (2009).
- ²³J. Chen, R. I. Dima, and D. Thirumalai, Allosteric communication in dihydrofolate reductase: Signaling network and pathways for closed to occluded transition and back, *J. Mol. Biol.* **374**, 250 (2007).
- ²⁴M. D. Vesper and B. L. de Groot, Collective dynamics underlying allosteric transitions in hemoglobin, *PLoS Comp. Biol.* **9**, e1003232 (2013).
- ²⁵F. Pontiggia, D. Pachov, M. Clarkson, J. Villali, M. Hagan, V. Pande, and D. Kern, Free energy landscape of activation in a signalling protein at atomic resolution, *Nat. Commun.* **6**, 7284 (2015).
- ²⁶Y. Zheng and Q. Cui, Multiple pathways and time scales for conformational transitions in apo-adenylate kinase, *J. Chem. Theory Comput.* **14**, 1716 (2018).
- ²⁷O. Bozovic, J. Ruf, C. Zanobini, B. Jankovic, D. Buhrke, P. J. M. Johnson, and P. Hamm, The Speed of Allosteric Signaling Within a Single-Domain Protein., *J. Phys. Chem. Lett.* **12**, 4262 (2021).
- ²⁸B. Buchli, S. A. Waldauer, R. Walser, M. L. Donten, R. Pfister, N. Bloechli, S. Steiner, A. Cafilisch, O. Zerbe, and P. Hamm, Kinetic response of a photoperturbed allosteric protein, *Proc. Natl. Acad. Sci. USA* **110**, 11725 (2013).
- ²⁹O. Bozovic, C. Zanobini, A. Gulzar, B. Jankovic, D. Buhrke, M. Post, S. Wolf, G. Stock, and P. Hamm, Real-time observation of ligand-induced allosteric transitions in a PDZ domain, *Proc. Natl. Acad. Sci. USA* **117**, 26031 (2020).
- ³⁰O. Bozovic, B. Jankovic, and P. Hamm, Sensing the allosteric force, *Nat. Commun.* **11**, 5841 (2020).
- ³¹O. Bozovic, B. Jankovic, and P. Hamm, Using azobenzene photocontrol to set proteins in motion, *Nat. Rev. Chem.* **6**, 112 (2022).
- ³²S. Buchenberg, V. Knecht, R. Walser, P. Hamm, and G. Stock, Long-range conformational transition in a photoswitchable allosteric protein: A molecular dynamics simulation study, *J. Phys. Chem. B* **118**, 13468 (2014).
- ³³S. Buchenberg, F. Sittel, and G. Stock, Time-resolved observation of protein allosteric communication, *Proc. Natl. Acad. Sci. USA* **114**, E6804 (2017).
- ³⁴P. H. Nguyen and G. Stock, Nonequilibrium molecular dynamics simulation of a photoswitchable peptide, *Chem. Phys.* **323**, 36 (2006).
- ³⁵D. A. Doyle, A. Lee, J. Lewis, E. Kim, M. Sheng, and R. MacKinnon, Crystal structures of a complexed and peptide-free membrane protein-binding domain: Molecular basis of peptide recognition by PDZ, *Cell* **85**, 1067 (1996).
- ³⁶E. Lindahl, M. J. Abraham, B. Hess, and D. van der Spoel, Gromacs 2020, Xenodo (2020).
- ³⁷V. Hornak, R. Abel, A. Okur, B. Strockbine, A. Roitberg, and C. Simmerling, Comparison of multiple Amber force fields and development of improved protein backbone parameters, *Proteins* **65**, 712 (2006).
- ³⁸R. B. Best and G. Hummer, Optimized molecular dynamics force fields applied to the helix-coil transition of polypeptides, *J. Phys. Chem. B* **113**, 9004 (2009).
- ³⁹K. Lindorff-Larsen, S. Piana, K. Palmo, P. Maragakis, J. L. Klepeis, R. O. Dror, and D. E. Shaw, Improved side-chain torsion potentials for the amber ff99sb protein force field., *Proteins* **78**, 1950 (2010).
- ⁴⁰F. Hoffmann, F. A. A. Mulder, and L. V. Schäfer, Predicting NMR relaxation of proteins from molecular dynamics simulations with accurate methyl rotation barriers, *J. Chem. Phys.* **152**, 084102 (2020).
- ⁴¹V. A. Lórenz-Fonfría and H. Kandori, Transformation of time-resolved spectra to lifetime-resolved spectra by maximum entropy inversion of the Laplace transform, *Appl. Spectrosc.* **60**, 407 (2006).
- ⁴²T. Nägele, R. Hoche, W. Zinth, and J. Wachtveitl, Femtosecond photoisomerization of cis-azobenzene, *Chem. Phys. Lett.* **272**, 489 (1997).
- ⁴³M. Ernst, S. Wolf, and G. Stock, Identification and validation of reaction coordinates describing protein functional motion: Hierarchical dynamics of T4 Lysozyme, *J. Chem. Theory Comput.* **13**, 5076 (2017).
- ⁴⁴M. Post, B. Lickert, G. Diez, S. Wolf, and G. Stock, Cooperative protein allosteric transition mediated by a fluctuating transmission network, *J. Mol. Bio.* **434**, 167679 (2022).
- ⁴⁵G. R. Bowman and P. L. Geissler, Equilibrium fluctuations of a single folded protein reveal a multitude of potential cryptic allosteric sites, *Proc. Natl. Acad. Sci. USA* **109**, 11681 (2012).
- ⁴⁶M. Ernst, F. Sittel, and G. Stock, Contact- and distance-based principal component analysis of protein dynamics, *J. Chem. Phys.* **143**, 244114 (2015).
- ⁴⁷G. Diez, D. Nagel, and G. Stock, Correlation-based feature selection to identify functional dynamics in proteins, *J. Chem. Theory Comput.* **18**, 5079 – 5088 (2022).
- ⁴⁸V. Traag, L. Waltman, and N. van Eck, From Louvain to Leiden: guaranteeing well-connected communities, *Sci. Rep.* **9**, 5233 (2019).
- ⁴⁹J. Murciano-Calles, C. Corbi-Verge, A. M. Candel, I. Luque, and J. C. Martinez, Post-translational modifications modulate ligand recognition by the third PDZ domain of the MAGUK protein PSD-95, *PLOS ONE* **9**, 1 (2014).
- ⁵⁰C. N. Chi, A. Bach, K. Stromgaard, S. Gianni, and P. Jemth, Ligand binding by PDZ domains, *Biofactors* **38**, 338 (2012).
- ⁵¹S. Mostarda, D. Gfeller, and F. Rao, Beyond the binding site: The role of the β_2 - β_3 loop and extra-domain structures in PDZ domains, *PLOS Comp. Bio.* **8**, 1 (2012).
- ⁵²A. Sethi, J. Eargle, A. A. Black, and Z. Luthey-Schulten, Dynamical networks in tRNA:protein complexes, *Proc. Natl. Acad. Sci. USA* **106**, 6620 (2009).
- ⁵³W. Stacklies, C. Seifert, and F. Graeter, Implementation of force distribution analysis for molecular dynamics simulations, *BMC Bioinform.* **12**, 101 (2011).

Supplementary Information: Nonequilibrium Modeling of the Elementary Step in PDZ3 Allosteric Communication

Ahmed A. A. I. Ali,^{*} Adnan Gulzar,^{*} Steffen Wolf, and Gerhard Stock[†]
Biomolecular Dynamics, Institute of Physics, University of Freiburg, 79104 Freiburg, Germany

(Dated: September 19, 2022)

METHODS

Molecular dynamics simulations

All MD simulations of PDZ3 were performed using the GROMACS v2020 software package[1] with a hybrid GPU-CPU acceleration scheme[2] and the Amber99*ILDN force field.[3–5] Force field parameters of the azobenzene photoswitch were previously reported in Ref. [6]. Protein-ligand structures were solvated with ca. 6000 TIP3P water molecules[7] in a dodecahedron box with a minimal image distance of 7 nm. 21 Na⁺ and 19 Cl⁻ were added to yield a charge-neutral system with a salt concentration of 0.15 M. All bonds involving hydrogen atoms were constrained using the LINCS algorithm[8], allowing for a time step of 2 fs. Long-range electrostatic interactions were computed by the Particle Mesh Ewald method[9], while the short-range electrostatic interactions were treated explicitly with the Verlet cutoff scheme. The minimum cutoff distance for electrostatic and van der Waals interactions was set to 1.4 nm. A temperature of 300 K was maintained via the Bussi thermostat[10] (aka velocity-rescale algorithm) with a coupling time constant of $\tau_T = 0.1$ ps. A pressure $P = 1$ bar was controlled using the pressure coupling method of Berendsen[11] with a coupling time constant of $\tau_P = 0.1$ ps.

The starting structure of the PDZ3 was taken from PDB entry 1TP5[12]. To generate initial structures for the MD simulations of α_3 -switched PDZ3, we first removed the last 13 residues (104-116) from the crystal structure, and the azobenzene photoswitch was then attached at positions 95 and 102.

These residues were first mutated to cysteins as in the experiment of Bozovic et al.[13] to provide covalent connection points. Similarly, to be consistent with the experiments, we considered a 5-mer peptide (KETWV). The five amino acid peptide is the shortest possible sequence, which still includes the five crucial amino acids for specific binding to the PDZ3 domain.[14]

For the equilibrium simulations, PDZ3 was minimized in both *cis* and *trans* conformations of photoswitch. Following NPT equilibration of both systems for 10 ns, systems were again equilibrated in NVT-ensemble for 100 ns. From the last 50 ns, 8 statistically independent structures (i.e., with different initial velocity distributions) were chosen for NVT runs of 5 μ s length each. In this way, we simulated both equilibrium systems for the cumulative time of 80 μ s each. For the nonequilibrium *cis-to-trans* simulations, we chose 100 statistically independent structures from last 50 ns of the NVT equilibration run of the *cis* state. Azobenzene photoswitching was performed by using potential-energy surface switching approach [15]. All 100 *cis-to-trans* nonequilibrium simulations were run for 1 μ s.

Gromacs tools *gmx mdat* and *gmx mindist* were employed to compute contact map, interresidue C_α -distances, and the number of contacts between various segments of PDZ2. Time-dependent distributions and mean values of any observables were calculated via an ensemble average over 100 nonequilibrium trajectories. We consider a contact to be formed when the average minimum distance between two residues is less than 0.45 nm.[16]

^{*} A. Ali and A. Gulzar contributed equally to this work.

[†] stock@physik.uni-freiburg.de

Calculations of NMR order parameters

To calculate order parameters, we performed 10 additional NVT simulations for wild-type PDZ3, **cis** and **trans** conformations of photoswitchable PDZ3. Force field Amber99SB*-ILDN with re-parameterization of methyl rotation barriers of Hoffmann[17] was used. MD simulations were performed for 200 ns, generating a cumulative time length of 2 μ s for each system. In order to improve the prediction of calculated order parameters, frames of trajectories were printed after every 1 ps. Order parameters were calculated using the methods of Chen[18] and Hoffmann[19]. The translational and rotational motions were removed in order to calculate only the internal time correlation functions (TCFs) for each methyl group.

$$C(\tau) = \langle P_2[\vec{\mu}(0) \cdot \vec{\mu}(\tau)] \rangle \quad (\text{S1})$$

P_2 is the second Legendre polynomial where

$$P_2(x) = \frac{1}{2}(3x^2 - 1), \quad (\text{S2})$$

and $\vec{\mu}(\tau)$ is the unit bond vector (C-H bond vector in case of methyl group), and $\langle \dots \rangle$ indicates averaging over all time step differences (τ).

Finally, the TCFs were then fitted to LS2 (two parameters fit) model of Lipari-Szabo[20]:

$$C_{LS2}(\tau) = S^2 + (1 - S^2) e^{-\frac{\tau}{\tau_f}}, \quad (\text{S3})$$

where $S^2 = S_f^2 S_{axis}^2$, with the order parameter of the symmetrical methyl rotation axis [21] S_{axis}^2 and S_f^2 :

$$S_f^2 = P_2(\cos \theta_{ij}) \cdot P_2(\cos \theta_{kl}) \quad (\text{S4})$$

where θ_{ij} is the angle between two C-H bond vectors in the methyl group. For a methyl group with ideal tetrahedral geometry, $\theta_{ij} = 109.5^\circ$ and $P_2(\cos \theta_{ij}) = -1/3$, we obtain $S_f^2 = 1/9$.

Contacts selection

To identify the contacts, we used 2.5×10^5 cis, 2.5×10^5 trans, and 5×10^5 NEQ frames to weight both equilibrium and nonequilibrium data equally. Moreover, we selected the contacts based on the following criteria:

- Minimal distance (d_{ij}) should be ≤ 0.45 nm between residues i 's and j 's non-hydrogen atoms.
- The two residues should be in contact for ≥ 10 % of the considered frames.
- $|i - j| > 2$ to neglect nearest and next to nearest neighbor residues.

These criteria resulted in 403 contact distances.

RESULTS

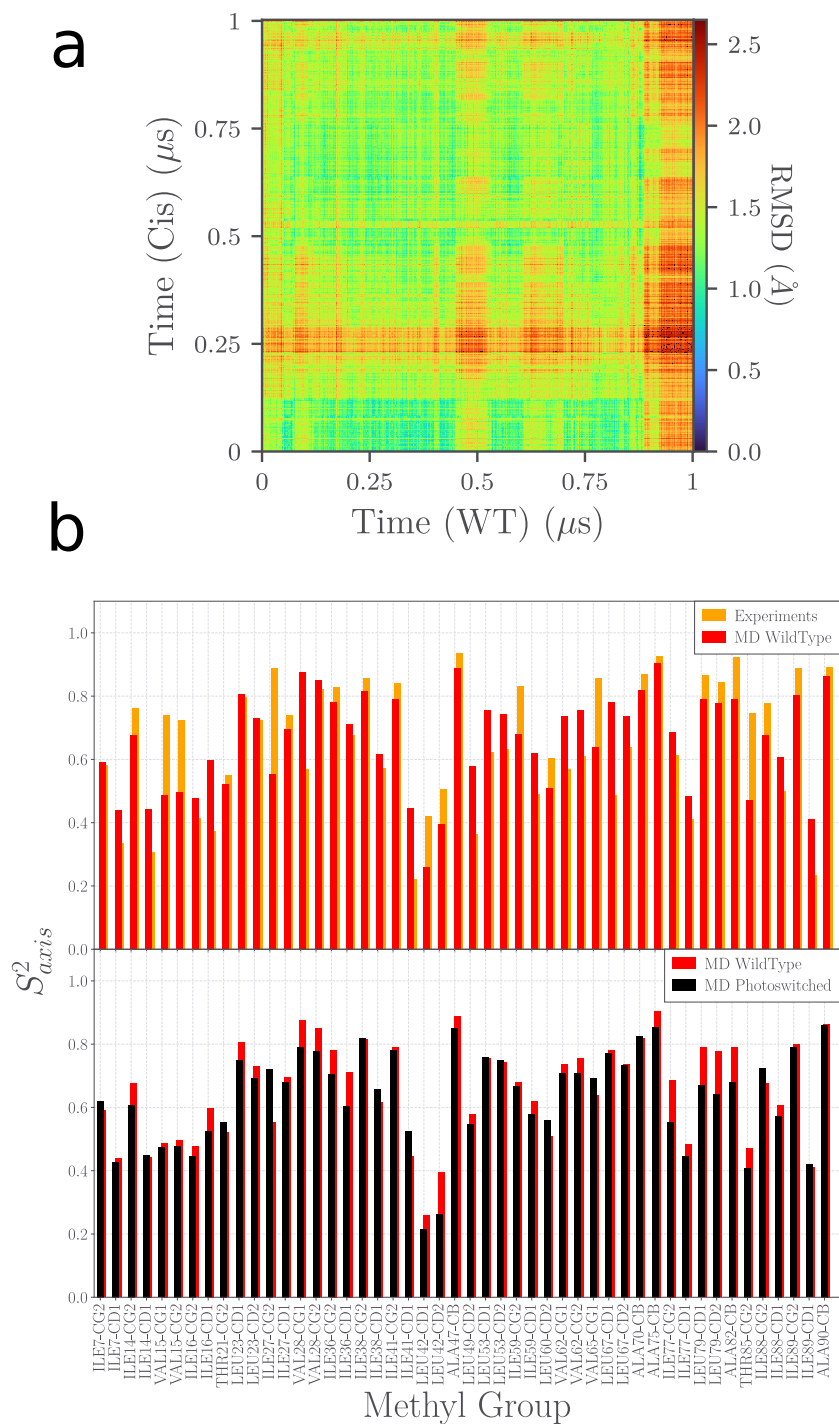


FIG. S1. (a) RMSD map between wild-type (WT) PDZ3 (x-axis) and cis-PDZ3 (y-axis) for a 1 μ s equilibrium trajectory. The RMSD was calculated for C_{α} atoms, excluding the ligand and the first 5 and the last 2 residues of the protein, because of their high flexibility. The reference structure was set as the first frame of the WT simulation. This matrix has an average RMSD value of 1.45 Å. (b) Bar chart between (top) experimental [22] and computational (WT PDZ3) results for S^2_{axis} . (bottom) Results for S^2_{axis} WT and photoswitched PDZ3 (cis) calculations.

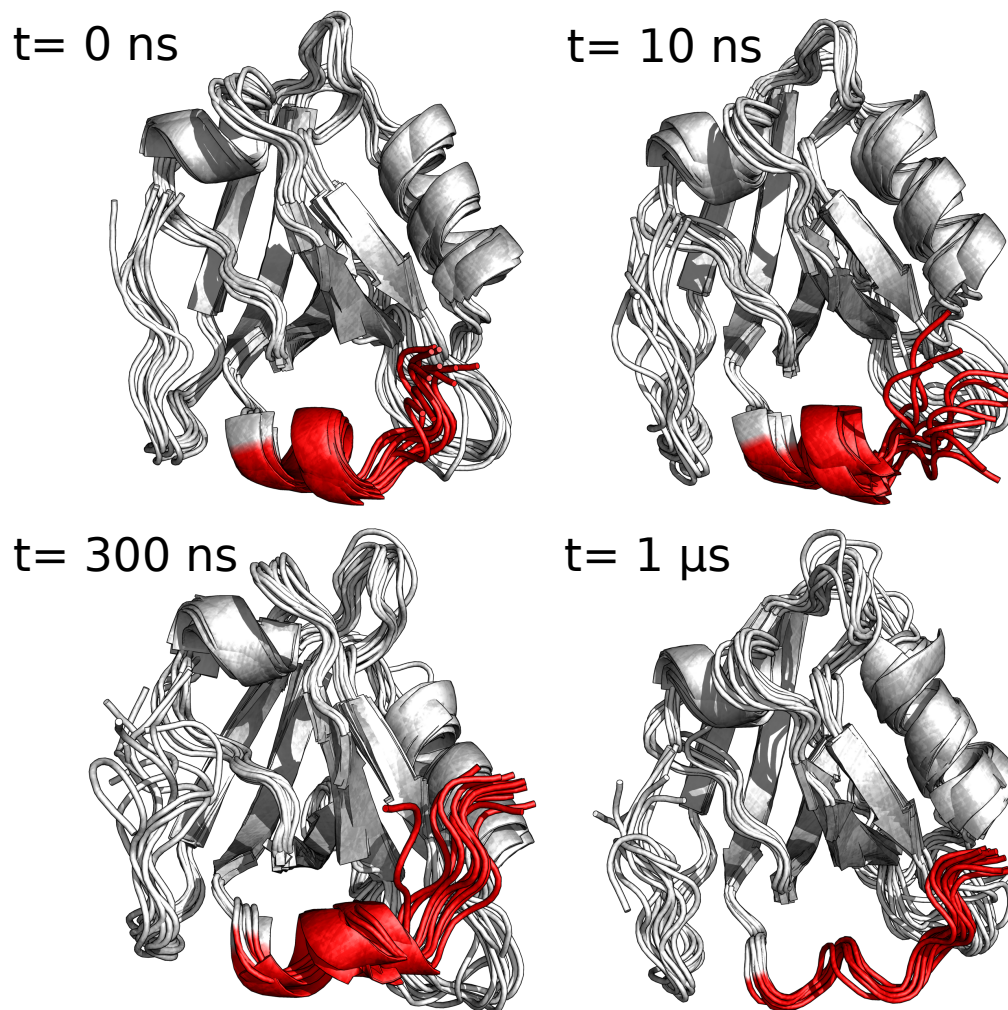


FIG. S2. Enforced unfolding of the α_3 -helix (red) of PDZ3, following cis-to-trans photoswitching of α_3 (see Fig. 1 of the main text). Shown are snapshots of 10 randomly chosen nonequilibrium MD trajectories at indicated simulation times.

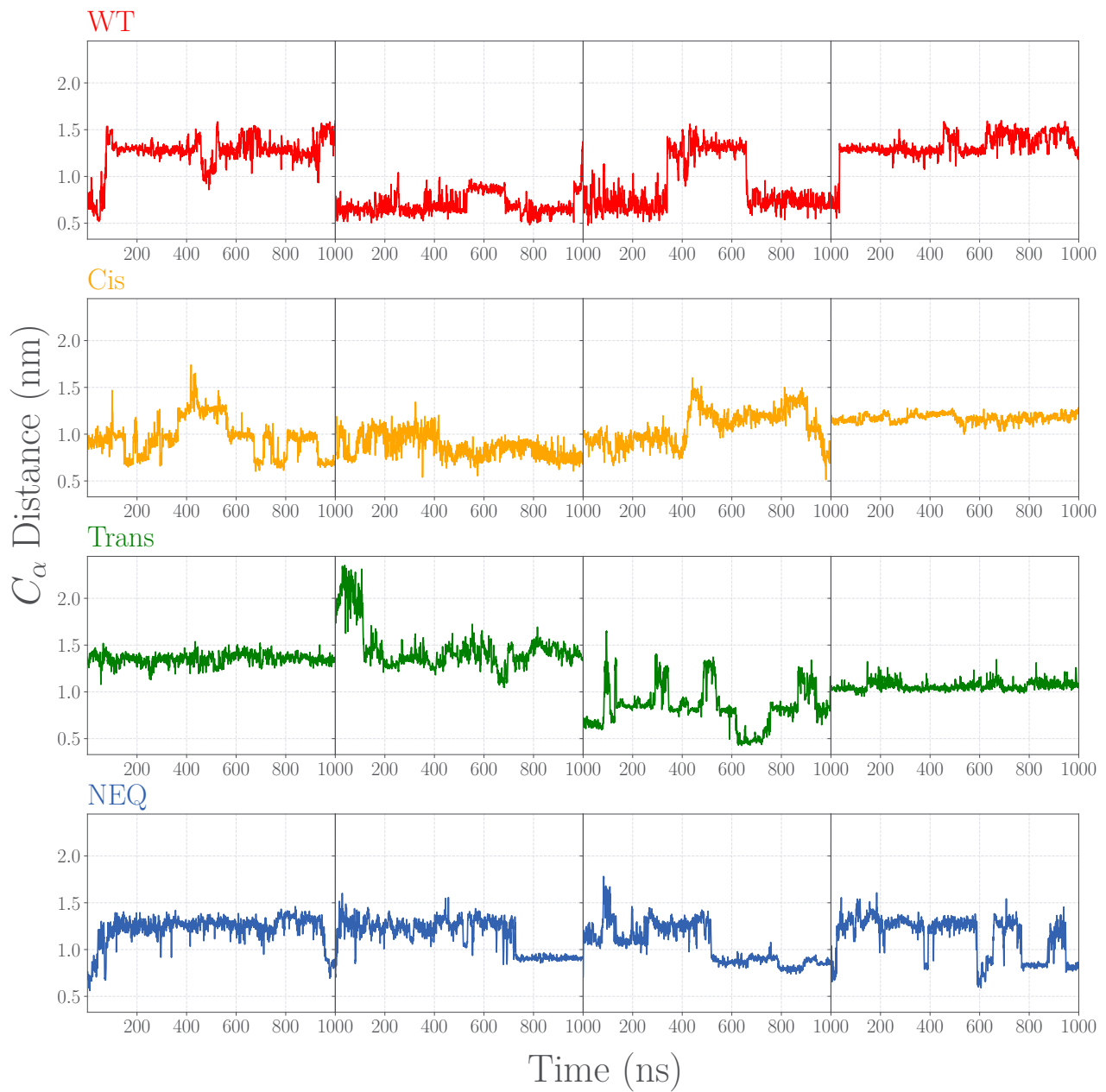


FIG. S3. Time evolution of C_α $d_{29,102}$ distance between α_3 and $\beta_2\beta_3$ obtained for wild-type, cis, trans and nonequilibrium systems. For smoothing a Gaussian filter with width $\sigma = 0.2$ ns was used.

TABLE S1. Coordinates of Leiden clusters 1 - 8 shown in Fig. 3 of the main text. Clusters with a star indicate coordinates (or mini-clusters with ≤ 3 coordinates) that are not a member of a main cluster but still exhibit moderate correlation with some of the main clusters.

Cluster Coordinates	
1	$r_{102,(-3)}, r_{28,102}, r_{39,102}, r_{28,101}, r_{97,102}, r_{101,(-4)}, r_{101,(-3)}, r_{94,102}, r_{103,(-4)}, r_{55,102},$ $r_{103,(-3)}$
1*	$r_{32,70}, r_{32,71}, r_{32,69}, r_{55,97}, r_{98,102}, r_{5,95}, r_{29,34}, r_{94,98}, r_{95,99}, r_{93,97}, r_{39,97}$
2	$r_{29,100}, r_{37,100}, r_{35,100}, r_{30,100}, r_{28,100}, r_{97,100}, r_{34,100}, r_{31,100}, r_{96,100}$
2*	$r_{97,101}, r_{96,99}, r_{100,103}, r_{99,102}$
3	$r_{35,69}, r_{35,68}, r_{33,69}, r_{34,69}, r_{35,67}, r_{33,70}, r_{34,68}, r_{58,68}, r_{33,71}, r_{35,70}, r_{59,68}, r_{33,68},$ $r_{29,71}, r_{36,79}$
3*	$r_{34,70}, r_{60,68}, r_{61,68}, r_{60,67}, r_{28,72}, r_{27,72}, r_{67,78}, r_{62,86}, r_{36,75}, r_{59,79}, r_{73,(-2)}, r_{76,(-1)},$ $r_{30,72}, r_{36,71}, r_{36,70}, r_{79,86}, r_{70,74}, r_{69,74}, r_{34,96}, r_{66,70}, r_{28,38}, r_{42,(-1)}, r_{30,34}, r_{28,35},$ $r_{31,73}, r_{30,36}, r_{30,70}, r_{30,35}, r_{67,79}$
4	$r_{28,(-4)}, r_{27,(-3)}, r_{29,(-4)}, r_{27,(-4)}, r_{28,(-3)}, r_{72,(-4)}$
4*	$r_{72,(-2)}, r_{27,(-2)}, r_{76,(-2)}, r_{72,(-3)}, r_{31,(-4)}, r_{39,(-3)}$
5	$r_{78,82}, r_{62,82}, r_{82,86}, r_{79,82}, r_{63,82}, r_{81,86}, r_{77,81}, r_{79,83}, r_{18,81}, r_{83,86}$
5*	$r_{63,81}, r_{82,85}, r_{80,83}, r_{62,78}, r_{63,78}, r_{59,62}$
6	$r_{21,25}, r_{20,(-1)}, r_{18,(0)}, r_{21,43}, r_{21,(-1)}, r_{21,45}, r_{21,24}, r_{24,(0)}, r_{22,(-1)}, r_{18,(-1)}, r_{21,42},$ $r_{18,82}, r_{21,46}, r_{18,83}, r_{18,86}$
6*	$r_{25,79}, r_{80,(0)}, r_{25,(0)}, r_{24,46}, r_{24,45}, r_{26,42}, r_{25,42}, r_{24,(-1)}, r_{27,(0)}, r_{17,85}, r_{25,(-2)}, r_{17,22},$ $r_{23,(0)}, r_{23,45}, r_{25,47}, r_{24,40}, r_{19,22}, r_{18,21}, r_{19,84}, r_{19,46}, r_{70,75}$
7	$r_{47,52}, r_{47,51}, r_{16,52}, r_{25,53}, r_{15,52}, r_{14,50}, r_{50,53}, r_{51,54}$
7*	$r_{23,47}, r_{12,54}, r_{47,50}, r_{52,57}, r_{41,48}, r_{12,91}$
8	$r_{1,95}, r_{2,95}, r_{1,98}, r_{2,51}, r_{1,51}, r_{1,102}, r_{2,98}, r_{2,52}, r_{3,54}, r_{2,102}, r_{1,100}, r_{1,48}, r_{3,95}, r_{2,94}, r_{2,53},$ $r_{2,54}, r_{2,97}$
8*	$r_{4,55}, r_{3,55}, r_{3,97}, r_{2,55}$

Cluster Coordinates

Noise $r_{29,35}, r_{34,58}, r_{3,92}, r_{31,72}, r_{31,71}, r_{30,71}, r_{29,72}, r_{25,59}, r_{27,59}, r_{76,(0)}, r_{36,72}, r_{27,75}, r_{27,76},$
 $r_{36,67}, r_{79,88}, r_{62,79}, r_{71,74}, r_{31,34}, r_{31,70}, r_{30,33}, r_{28,36}, r_{29,36}, r_{35,58}, r_{36,57}, r_{36,58}, r_{36,59},$
 $r_{73,(-4)}, r_{40,(-3)}, r_{40,(-1)}, r_{26,(-3)}, r_{26,(-1)}, r_{78,81}, r_{23,79}, r_{27,79}, r_{67,74}, r_{74,77}, r_{71,75}, r_{73,77},$
 $r_{73,76}, r_{65,78}, r_{67,75}, r_{62,67}, r_{72,76}, r_{72,75}, r_{80,(-1)}, r_{80,(-2)}, r_{76,80}, r_{76,79}, r_{77,80}, r_{79,(0)},$
 $r_{75,78}, r_{75,79}, r_{74,78}, r_{59,67}, r_{61,67}, r_{66,69}, r_{61,89}, r_{67,70}, r_{26,37}, r_{27,38}, r_{27,39}, r_{27,37}, r_{26,38},$
 $r_{26,39}, r_{28,37}, r_{28,39}, r_{24,47}, r_{26,(-2)}, r_{25,(-1)}, r_{17,46}, r_{17,23}, r_{16,25}, r_{18,22}, r_{22,(0)}, r_{21,(0)},$
 $r_{23,46}, r_{18,46}, r_{22,46}, r_{16,23}, r_{18,79}, r_{18,80}, r_{18,23}, r_{25,40}, r_{26,40}, r_{24,41}, r_{24,42}, r_{42,45}, r_{45,48},$
 $r_{16,50}, r_{46,50}, r_{45,49}, r_{46,49}, r_{44,49}, r_{48,51}, r_{61,65}, r_{60,65}, r_{61,64}, r_{60,66}, r_{61,66}, r_{62,65}, r_{63,86},$
 $r_{63,85}, r_{63,87}, r_{61,87}, r_{62,87}, r_{4,92}, r_{4,54}, r_{1,4}, r_{2,5}, r_{5,54}, r_{9,54}, r_{54,92}, r_{5,9}, r_{12,53}, r_{41,47},$
 $r_{12,52}, r_{53,57}, r_{54,57}, r_{57,90}, r_{47,53}, r_{53,90}, r_{57,91}, r_{57,92}, r_{12,92}, r_{56,92}, r_{57,93}, r_{56,94}, r_{56,93},$
 $r_{56,91}, r_{55,92}, r_{41,55}, r_{41,54}, r_{41,53}, r_{25,41}, r_{38,41}, r_{38,55}, r_{38,56}, r_{38,97}, r_{39,55}, r_{40,55}, r_{37,57},$
 $r_{38,57}, r_{38,54}, r_{95,98}, r_{28,97}, r_{56,97}, r_{34,99}, r_{37,99}, r_{37,93}, r_{37,56}, r_{34,37}, r_{37,97}, r_{94,97}, r_{37,58},$
 $r_{58,96}, r_{93,96}, r_{37,96}, r_{8,94}, r_{7,94}, r_{6,95}, r_{8,95}, r_{5,94}, r_{5,92}, r_{7,92}, r_{6,94}, r_{8,93}, r_{8,92}, r_{9,92}, r_{14,90},$
 $r_{14,89}, r_{12,88}, r_{13,52}, r_{14,52}, r_{14,53}, r_{13,87}, r_{13,88}, r_{14,87}, r_{14,88}, r_{23,88}, r_{25,88}, r_{61,88}, r_{62,88},$
 $r_{53,88}, r_{59,88}, r_{16,88}, r_{16,46}, r_{16,47}, r_{23,86}, r_{16,53}, r_{11,60}, r_{11,89}, r_{11,90}, r_{12,89}, r_{12,90}, r_{10,90},$
 $r_{10,91}, r_{9,91}, r_{11,91}, r_{58,93}, r_{60,91}, r_{58,89}, r_{59,90}, r_{60,90}, r_{58,90}, r_{59,89}, r_{60,89}, r_{58,91}, r_{25,38},$
 $r_{38,53}, r_{27,36}, r_{38,59}, r_{44,48}, r_{43,48}, r_{42,48}, r_{14,86}, r_{15,86}, r_{15,87}, r_{15,85}, r_{16,85}, r_{16,86}, r_{17,84},$
 $r_{18,84}, r_{16,84}, r_{12,57}, r_{13,89}, r_{95,102}$

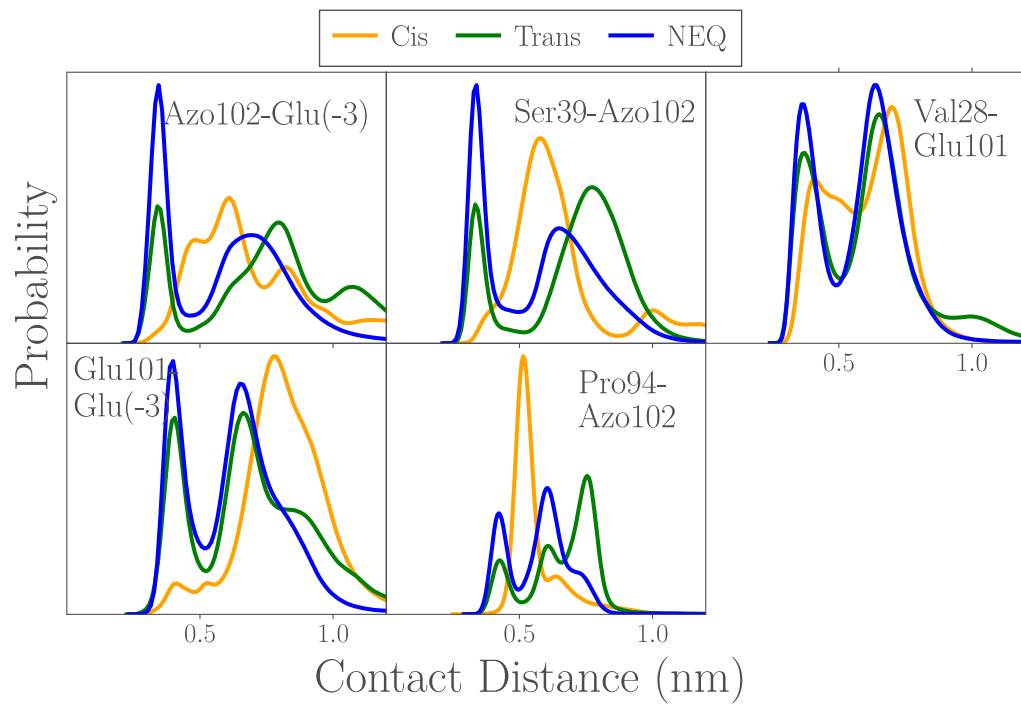
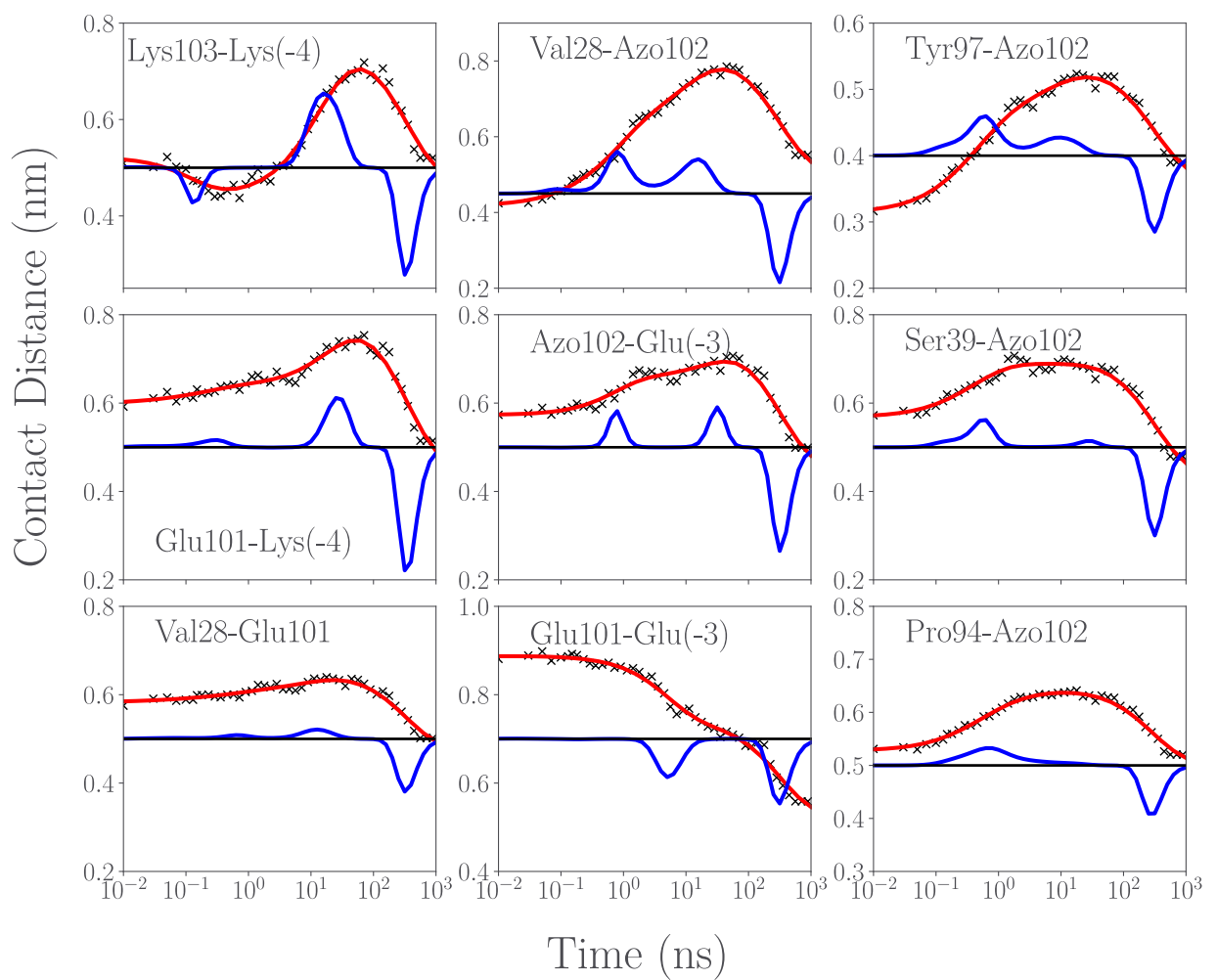
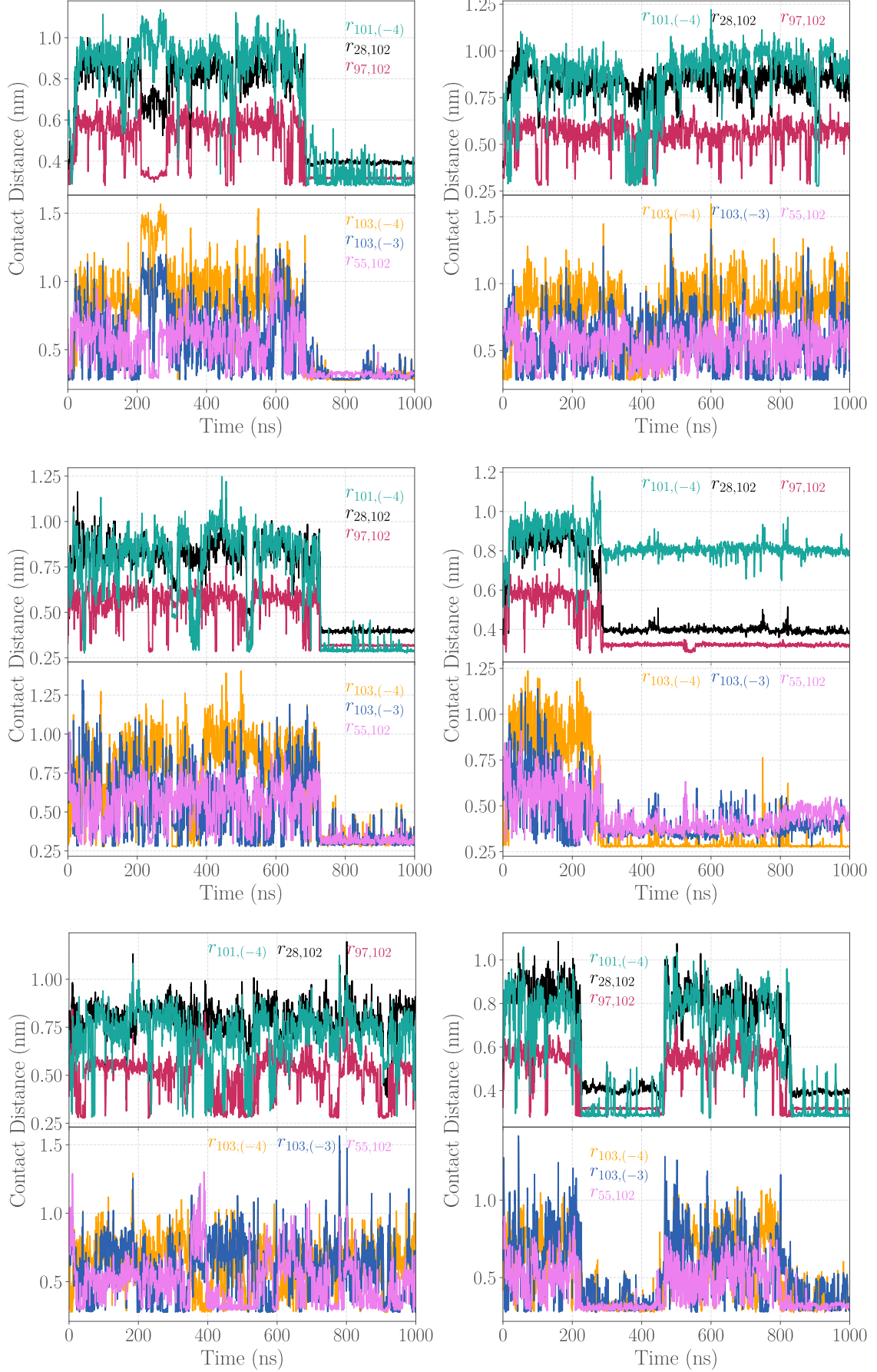
a**b**

FIG. S4. (a) Probability distribution of 5 contact distances from cluster 1. (b) Timescale analysis of 9 contact distances from cluster 1, using nonequilibrium data.

FIG. S5. Time evolution of selected contacts that undergoes a nonequilibrium evolution from *cis* to *trans*. For smoothing a Gaussian filter with width $\sigma = 0.2$ ns was used.





-
- [1] M. J. Abraham, T. Murtola, R. Schulz, S. Páll, J. C. Smith, B. Hess, and E. Lindahl, “Gromacs: High performance molecular simulations through multi-level parallelism from laptops to supercomputers”, *SoftwareX* **1-2**, 19–25 (2015).
 - [2] S. Pronk, S. Páll, R. Schulz, P. Larsson, P. Bjelkmar, R. Apostolov, M. R. Shirts, J. C. Smith, P. M. Kasson, D. van der Spoel, B. Hess, and E. Lindahl, “Gromacs 4.5: a high-throughput and highly parallel open source molecular simulation toolkit.”, *Bioinformatics (Oxford, England)* **29**, 845–54 Apr (2013).
 - [3] V. Hornak, R. Abel, A. Okur, B. Strockbine, A. Roitberg, and C. Simmerling, “Comparison of multiple amber force fields and development of improved protein backbone parameters.”, *Proteins* **65**, 712–25 Nov (2006).
 - [4] R. B. Best and G. Hummer, “Optimized molecular dynamics force fields applied to the helix-coil transition of polypeptides.”, *The journal of physical chemistry. B* **113**, 9004–15 Jul (2009).
 - [5] K. Lindorff-Larsen, S. Piana, K. Palmo, P. Maragakis, J. L. Klepeis, R. O. Dror, and D. E. Shaw, “Improved side-chain torsion potentials for the amber ff99sb protein force field.”, *Proteins* **78**, 1950–8 Jun (2010).
 - [6] C. Zanobini, O. Bozovic, B. Jankovic, K. L. Koziol, P. J. M. Johnson, P. Hamm, A. Gulzar, S. Wolf, and G. Stock, “Azidohomoalanine: A minimally invasive, versatile, and sensitive infrared label in proteins to study ligand binding”, *The Journal of Physical Chemistry B* **122**, 10118–10125 (2018).
 - [7] W. Jorgensen, J. Chandrasekhar, J. Madura, R. Impey, and M. Klein, “Comparison of simple potential functions for simulating liquid water”, *The Journal of Chemical Physics* **79**, 926–935 (1983).
 - [8] B. Hess, “P-lincs: A parallel linear constraint solver for molecular simulation”, *Journal of chemical theory and computation* **4**, 116–122 (2008).
 - [9] U. Essmann, L. Perera, M. L. Berkowitz, T. Darden, H. Lee, and L. G. Pedersen, “A smooth particle mesh ewald method”, *The Journal of Chemical Physics* **103**, 8577–8593 (1995).
 - [10] G. Bussi, D. Donadio, and M. Parrinello, “Canonical sampling through velocity rescaling.”, *The Journal of chemical physics* **126**, 014101 Jan (2007).
 - [11] H. J. Berendsen, J. P. M. Postma, W. F. van Gunsteren, A. DiNola, and J. Haak, “Molecular dynamics with coupling to an external bath”, *The Journal of chemical physics* **81**, 3684 (1984).
 - [12] D. Saro, P. Martin, J. Vickrey, A. Griffin, L. Kovari, and M. Spaller, “Structure of the third pdz domain of psd-95 protein complexed with kktptv peptide ligand”, *To be Publ.*
 - [13] O. Bozovic, J. Ruf, C. Zanobini, B. Jankovic, D. Buhrke, P. J. M. Johnson, and P. Hamm, “The speed of allosteric signaling within a single-domain protein”, *The Journal of Physical Chemistry Letters* **12**, 4262–4267 (2021), PMID: 33904738.
 - [14] D. Saro, T. Li, C. Rupasinghe, A. Paredes, N. Caspers, and M. R. Spaller, “A thermodynamic ligand binding study of the third pdz domain (pdz3) from the mammalian neuronal protein psd-95.”, *Biochemistry* **46**, 6340–52 May (2007).
 - [15] P. H. Nguyen and G. Stock, “Nonequilibrium molecular dynamics simulation of a photoswitchable peptide”, *Chemical Physics* **323**, 36–44 (2006).
 - [16] M. Ernst, F. Sittel, and G. Stock, “Contact- and distance-based principal component analysis of protein dynamics”, *The Journal of Chemical Physics* **143**, 244114 (2015).
 - [17] F. Hoffmann, F. A. Mulder, and L. V. Schäfer, “Accurate methyl group dynamics in protein simulations with amber force fields”, *The Journal of Physical Chemistry B* **122**, 5038–5048 (2018).
 - [18] P.-c. Chen, M. Hologne, O. Walker, and J. Hennig, “Ab initio prediction of nmr spin relaxation parameters from molecular dynamics simulations”, *Journal of Chemical Theory and Computation* **14**, 1009–1019 (2018).
 - [19] F. Hoffmann, F. A. A. Mulder, and L. V. Schäfer, “Predicting nmr relaxation of proteins from molecular dynamics simulations with accurate methyl rotation barriers”, *The Journal of Chemical Physics* **152**, 084102 (2020).
 - [20] G. Lipari and A. Szabo, “Model-free approach to the interpretation of nuclear magnetic resonance relaxation in macromolecules. 1. theory and range of validity”, *Journal of the American Chemical Society* **104**, 4546–4559 (1982).
 - [21] L. E. Kay and D. Torchia, “The effects of dipolar cross correlation on ^{13}C methyl-carbon t1, t2, and noe measurements in macromolecules”, *Journal of Magnetic Resonance (1969)* **95**, 536–547 (1991).
 - [22] C. M. Petit, J. Zhang, P. J. Sapienza, E. J. Fuentes, and A. L. Lee, “Hidden dynamic allostery in a pdz domain.”, *Proceedings of the National Academy of Sciences of the United States of America* **106**, 18249–54 Oct (2009).